This article has been accepted for publication in a future issue of this journal, but has not been fully edited. Content may change prior to final publication. Citation information: DOI 10.1109/TSTE.2020.2992960, IEEE Transactions on Sustainable Energy

Optimal Energy Storage Allocation for Mitigating the Unbalance in Active Distribution Network via Uncertainty Quantification

Han Wang, *Student Member*, *IEEE*, Zheng Yan, Mohammad Shahidehpour, *Fellow*, *IEEE*, Quan Zhou, *Senior Member*, *IEEE*, and Xiaoyuan Xu, *Member*, *IEEE*

***Abstract*—Voltage unbalance (VU) in an active distribution network (ADN) could result in increased network losses and even system instability. The additional uncertainties embedded in ADN might lead to serious VU problems with the proliferation of single-phase distributed energy resources (DERs). This paper proposes a two-stage uncertainty quantification and unbalance mitigation (UQUM) framework to cope with the corresponding VU problems and quantify and mitigate the impacts of variable DERs on VU. In Stage one, the global sensitivity analysis based on the Rosenblatt transformation (RT-based GSA) method is proposed to quantify the impacts of nonlinearly correlated DERs with tail dependence on VU. The RT-GSA method can identify critical DERs with significant impacts on VU. In Stage two, the joint allocations of fixed and mobile energy storage devices (ESDs) are considered in which an optimal mitigation strategy is proposed to alleviate VU and effectively compensate the critical DER fluctuations (identified in Stage one). Based on the given DER data and the available ESD capacity, the effectiveness of the proposed UQUM framework is verified in a 123-bus three-phase unbalanced ADN and the corresponding results are discussed.**

***Index Terms*—Active distribution network, uncertainty, global sensitivity analysis, energy storage devices, probabilistic voltage unbalance mitigation.**

NOMENCLATURE

A. *Acronyms:*

VU	Voltage unbalance
DER	Distributed energy resource
ADN	Active distribution network
VUF	Voltage unbalance factor
ESD	Energy storage device
DS	Dependent structure
PDF	Probability density function
CDF	Cumulative distribution function
LCC	Linear correlation coefficient
GSA	Global sensitivity analysis
FSI	First-order sensitivity index
USI	Uncorrelated sensitivity index
CSI	Correlated sensitivity index
FESD	Fixed energy storage device
MESD	Mobile energy storage device

B. *Parameters:*

$f_l(x_l)$	PDF of x_l (l=1,…,n)
n	Number of input variables in $\boldsymbol{X}$
$c_{i,i+j\|\boldsymbol{i}}$	PDF of bivariate pair-copula
$C_{i,r\|(\sim r,\boldsymbol{i})}$	CDF of bivariate pair-copula
D_Y	Variance of Y
g_0	Mean of Y
$\boldsymbol{X}_a^{(k)}$	Sample satisfying joint PDF $f(\boldsymbol{X})$
$\boldsymbol{X}_b^{(k)}$	Sample satisfying conditional PDF $f(x_i, \boldsymbol{x}_{(\sim i)}\|x_i)$
N_s	Sample size for FSI estimation using MCS
$F_1(x_1)$	CDF of x_1
$f(x_i \mid \boldsymbol{x}_i)$	Conditional PDF of x_i
$F_{i\|\boldsymbol{i}}(x_i \mid \boldsymbol{x}_i)$	Conditional CDF corresponding to $f(x_i\|\boldsymbol{x}_i)$
T	Terminal time index in the time window [1, T]
η_c	Charging efficiency of ESD
η_{disc}	Discharging efficiency of ESD
SOC_{min}	Minimal allowed State-of-charge of ESD
SOC_{max}	Maximal allowed State-of-charge of ESD
ΔP_{max}^{c}	Maximal charging power of ESD
ΔP_{max}^{disc}	Maximal discharging power of ESD
N	Number of scenes
τ	Initial State-of-charge of ESD in mth scene

C. *Variables:*

V_-	Negative sequence voltage component
V_+	Positive sequence voltage component
V_{ab}, V_{bc}, V_{ca}	Line to line voltages
$\boldsymbol{X}$	Vector of input variables with (x_1,…,x_n)
$\boldsymbol{x_i}$	Vector of input variables with (x_1,…,x_{i-1})
$\boldsymbol{i}$	Vector of indices for $\boldsymbol{x_i}$ with (1,…,i-1)
$x_{r,\boldsymbol{i}}$	Arbitrary input variable selected from $\boldsymbol{x_i}$
$\boldsymbol{x}_{(\sim r,\boldsymbol{i})}$	Other input variables in $\boldsymbol{x_i}$ excluding $x_{r,\boldsymbol{i}}$
Y	Output variable with Y=$g(\boldsymbol{X})$
$\bar{\boldsymbol{x}}_{(\sim i)}$	Input variables satisfying PDF $f(x_i, \boldsymbol{x}_{(\sim i)}\|x_i)$
$P_{m,t}^{DER_i}$	Power injection of DER$_i$ after allocating ESD at time t in mth scene
$P_{m,t}^{D}$	Power injection of DER$_i$ before allocating ESD at time t in mth scene
$\bar{P}_m$	Mean of DER$_i$ power injection over the time window [1, T] in mth scene
$\Delta P_{m,t}^{c}$	ESD charging power at time t in mth scene
$\Delta P_{m,t}^{disc}$	ESD discharging power at time t in mth scene
$u_{m,t}^{c}$	Binary variable standing for the charging status of ESD at time t in mth scene
$u_{m,t}^{disc}$	Binary variable standing for the discharging status of ESD at time t in mth scene
$SOC_{m,t}$	State-of-charge of ESD at time t in mth scene

This work was supported by the National Key Research and Development Program of China (No. 2017YFB0902800). H. Wang, Z. Yan, and X. Xu are with the School of Electronic Information and Electrical Engineering, Shanghai Jiao Tong University in Shanghai, 200240, China (e-mail: wanghan9894@sjtu.edu.cn; xuxiaoyuan@sjtu.edu.cn; yanz@sjtu.edu.cn). M. Shahidehpour, and Q. Zhou are with the Electrical and Computer Engineering Department, Illinois Institute of Technology in Chicago (E-mail: ms@iit.edu, qzhou15@hawk.iit.edu). M. Shahidehpour is also with the Renewable Energy Research Group, King Abdulaziz University, Jeddah, Saudi Arabia

I. Introduction

VOLTAGE unbalance (VU) in distribution network are usually caused by unevenly distributed single-phase loads and asymmetrical line impedances, which would result in increased network losses and even system instability [1]-[4]. With the proliferation of distributed energy resources (DERs), VU in the active distribution network (ADN) will further deteriorate because of the single-phase integrated DERs, e.g., rooftop photovoltaic (PV) units [5], [6]. To guarantee the stable and reliable operation of distribution network, the International Electrotechnical Commission (IEC) suggests the voltage unbalance factor (VUF) should be limited within 2% [3]. Ref. [7] illustrates that the stipulated limit for VU in Malaysia has gradually become a major obstacle for promoting the accommodation of PVs. Therefore, it is crucial to mitigate VU in ADN with a high penetration of variable DERs.

Various approaches have been proposed to mitigate VU in power systems. In [8], static transfer switches were utilized to alleviate the VU by dynamically switching of residential loads between different phases. In [9], an optimization approach was proposed to mitigate the system unbalance and reduce the power losses by rearranging distribution transformer phases. Recently, electric vehicles (EVs) were utilized to mitigate the VU in low voltage networks by managing charging and discharging of EVs [10]. In addition to the listed methods for mitigating the unbalance at demand-side, inverter-interfaced DERs have been utilized to reduce VU. In [11], PV units and EVs were combined to realize VU mitigation considering PV power generation and charging patterns of EVs. In [12]-[14], various control schemes for inverters were presented to alleviate VU by injecting negative- and zero-sequence currents. Furthermore, single-phase energy storage device (ESD) is a viable solution to mitigate VU and improve voltage quality [7], [15]-[18]. The earlier VU mitigation studies were developed by using deterministic methods without considering uncertainties. The increasing penetration of variable DERs can significantly affect VU in ADN [19].

Considering ADN uncertainties, probabilistic methods associated with VU have attracted extensive attentions. In [19], probabilistic VUF estimation in distribution networks was offered considering variable unbalanced loads. In [20], probabilistic load flow and sensitivity analyses were performed to analyze the influences of variable loads on VU. In [21], the statistical VU estimation was proposed using distribution network state estimations. In [22], deterministic and stochastic methods were combined to derive VUF statistics. However, there are mainly three issues which are not well addressed in existing works, including 1) high penetration of DERs with correlated uncertainties [19]-[22]; 2) impacts of uncertainties on VU instead of only estimating VUF statistics; 3) probability property of correlated DERs in VU mitigation strategies. This paper focuses on addressing the above three issues and the proposed contributions are summarized as follows.

1. A two-stage uncertainty quantification and unbalance mitigation (UQUM) framework is proposed to quantify and mitigate the impacts of variable DERs on VU in three-phase ADN. The critical DERs which have significant impacts on VU are identified in Stage one and effectively guide the allocation of ESDs to mitigate VU in Stage two.
2. The global sensitivity analysis based on Rosenblatt transformation (RT-based GSA) method is proposed to quantify the impacts of variable DERs on the probabilistic voltage unbalance factor (PVUF). The derived GSA indices can identify critical DERs. Different from the studies in [23]-[25] and our previous studies in [26]-[29], DERs with complex dependent structure (DS) including nonlinear correlations and tail dependence are considered in the proposed RT-based GSA.
3. The joint allocation of fixed and mobile ESDs is proposed in Stage two to alleviate VU by using the optimal mitigation strategy, which can effectively compensate the fluctuations of critical DER power injections identified in Stage one.

The rest of this paper is organized as follows: A two-stage UQUM framework in three-phase ADN is established in Section II. The uncertainty quantification with RT-based GSA method is developed as Stage one in Section III. The unbalance mitigation based on the optimal mitigation strategy with ESDs is presented as Stage two in Section IV. Simulation results are shown in Section V, followed by the conclusion in Section VI.

II. Problem Formulation

In this section, PVUF represents the impacts of uncertainties on VU in the three-phase ADN. Then, a two-stage UQUM framework is proposed to quantify and mitigate the impacts of variable DERs on VU.

A. PVUF

In a three-phase ADN, VUF is a widely used index to evaluate the degree of VU, which is defined as:

$$\mathrm{VUF} = \frac{V_-}{V_+} \times 100\% = \gamma(V_{ab}, V_{bc}, V_{ca}) \tag{1}$$

Considering uncertainties (e.g., intermittent DER power injection) injected into ADN, VUF features probabilistic characteristics. To investigate the impacts of uncertainties on VUF, uncertainty propagation is introduced to exhibit the input-output statistical relationship between variable DERs and PVUF. First, DER data are collected to establish the probability models of DER power output, which is the process of uncertainty modeling for DERs. Then, variable DER power output is injected into the ADN as $\boldsymbol{X}$ and uncertainties in $\boldsymbol{X}$ are propagated to VUF. Finally, VUF statistics are derived and analyzed including means, variances, probability density functions (PDFs), and cumulative distribution functions (CDFs). Based on the process of uncertainty propagation, PVUF is stated as:

$$\mathrm{VUF}_{\boldsymbol{X}} = \gamma(V_{ab}(\boldsymbol{X}), V_{bc}(\boldsymbol{X}), V_{ca}(\boldsymbol{X})) = \zeta(\boldsymbol{X}) \tag{2}$$

For the PVUF calculation in (2), three-phase voltages are derived by solving a probabilistic three-phase unbalanced load flow in ADN [22].

B. Model Assumptions

Before introducing the proposed UQUM framework, the assumptions of our present work are given as follows:

1. In this paper, the proposed two-stage UQUM framework is applied to alleviate VU which would occur in a future time period considering the uncertainties of DERs. The identification of critical DERs in Stage one and the allocation of ESDs in Stage two would be completed before the studied time window.

This article has been accepted for publication in a future issue of this journal, but has not been fully edited. Content may change prior to final publication. Citation information: DOI 10.1109/TSTE.2020.2992960, IEEE Transactions on Sustainable Energy

2. The amounts and locations of DERs integrated into the three-phase ADN have been determined before the proposed UQUM framework is applied. Also, the probability models of correlated DERs are established based on the historical data in the studied time window.
3. The ESDs including fixed ESDs (FESDs) and mobile ESDs (MESDs) are only allocated at DER buses in the studied three-phase ADN, which are controlled by the system operator. The FESD is connected to several DER buses and would be allocated at a certain DER bus by closing the corresponding switch, which is defined as the shared FESD in this paper. The MESDs can be flexibly allocated at any DER buses and the uncertainty of MESDs involved in the movement is ignored. Moreover, the MESDs are assumed to have moved to the critical DER buses in advance because the reserved time for MESD scheduling is enough within the ADN area.
4. The capacity of FESDs and MESDs is known before allocating the ESDs and developing the optimal mitigation strategy.

C. Proposed UQUM Framework

Based on (2), the PVUF variation can be affected by the variable DER power injections through uncertainty propagation in ADN. With the proliferation of DERs, the corresponding uncertainties will increase the risk of exceeding the stipulated VUF limit (2% in this paper) in the ADN operation. In this paper, we focus on how to effectively reduce the impacts of variable DER power injections on VU in ADN, mainly considering the following two aspects:

1. *Identify critical DERs for VU:* In ADN, only a small proportion of DERs have significant impacts on VU. To realize precise and effective allocations of devices for mitigating the unbalance, it is crucial to quantify any impacts of DERs with complex correlations on VU and identify critical DERs, which is overlooked in the existing literature.
2. *Mitigate VU using ESDs:* The ESD operation strategy has significant impacts on VU when ESDs are used to compensate fluctuations of DER power injections [15], [16]. The ESD operation strategy should be optimized to mitigate VU in ADN, especially when available ESDs are limited.

Accordingly, a two-stage UQUM framework is proposed to quantify and mitigate the impacts of variable DERs on VU as shown in Fig. 1. In the proposed UQUM framework, the critical DERs which have significant impacts on VU are identified in Stage one and effectively guide the allocation of ESDs to mitigate VU in Stage two. Specifically, in Stage one, the RT-based GSA method is proposed to quantify the impacts of variable DERs on PVUF. The spatial and temporal correlations among DERs are captured by using complex DS. Based on the ranking of GSA indices, critical DERs with significant impacts on VU are identified. In Stage two, ESDs with optimal mitigation strategy are allocated at critical DER buses to compensate any fluctuations in DER power injections. Thus, the VU in ADN would be alleviated and the risk of exceeding VUF limit would be decreased. The integrated locations of ESDs in Stage two are determined by the results of uncertainty quantification in Stage one. Stages one and two in the proposed UQUM framework will be further elaborated on in Sections III and IV, respectively.

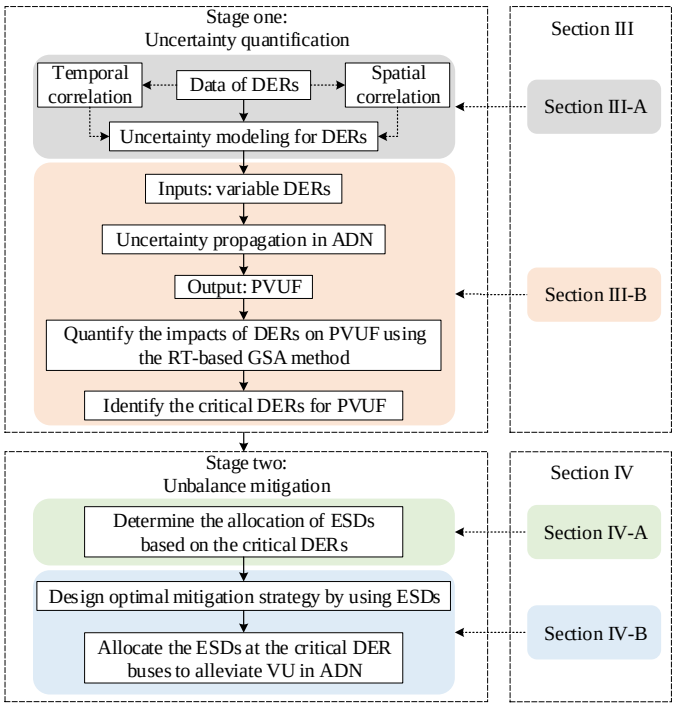

Fig. 1. Proposed two-stage UQUM framework in ADN.

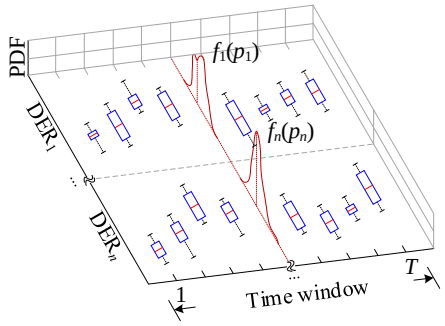

Fig. 2. Uncertainty modeling for DERs with spatial and temporal correlations ($f_i(p_i)$ is the PDF of DER_i (i=1,…,n) power output in the time window).

III. Stage One: Uncertainty Quantification

In this section, uncertainty modeling for spatially and temporally correlated DERs is presented. Then, the RT-based GSA method is proposed to quantify the impacts of variable DER power injection on VU. Utilizing the derived RT-GSA indices, critical DERs are identified which can guide the ESD allocations in Stage two.

A. Data-based Uncertainty Modeling for Correlated DERs

Through uncertainty modeling, we establish the probability models of DER power output and capture spatial and temporal correlations among DERs. In Fig. 2, there are n DERs and T time instants in a time window. Assume that δ observations of DER output power are collected at each time instant. Thus, the dataset of each DER is obtained including $M=T\times\delta$ observations. Utilizing the data, PDFs of DER power outputs can be established using a non-parameter kernel density estimation. Then, various DSs can be used to capture spatial and temporal correlations among DERs as follows:

1) Linear correlation coefficient and Gaussian copula: The linear correlation coefficient (LLC) and Gaussian copula are the

same to depict the correlations among input variables when the Nataf transformation is applied [30]. For n input variables $\boldsymbol{X}=(x_1,\ldots,x_n)$, the LLC matrix $\boldsymbol{\rho}$ of $\boldsymbol{X}$ is stated as:

$$\boldsymbol{\rho}=\begin{bmatrix}1 & \rho_{12} & \cdots & \rho_{1n}\\ \rho_{21} & 1 & \cdots & \rho_{2n}\\ \vdots & \vdots & \ddots & \vdots\\ \rho_{n1} & \rho_{n2} & \cdots & 1\end{bmatrix} \tag{3}$$

Let $\boldsymbol{X}_i^{(M)}=(x_i^{(1)},\ldots,x_i^{(M)})$ and $\boldsymbol{X}_j^{(M)}=(x_j^{(1)},\ldots,x_j^{(M)})$ denote M samples of x_i and x_j in a dataset, respectively. The correlation coefficient ρ_{ij} can be estimated by:

$$\hat{\rho}_{ij}=\frac{\sum_{m=1}^{M}\left(x_i^{(m)}-\frac{1}{M}\sum_{k=1}^{M}x_i^{(k)}\right)\left(x_j^{(m)}-\frac{1}{M}\sum_{k=1}^{M}x_j^{(k)}\right)}{\sqrt{\sum_{m=1}^{M}\left(x_i^{(m)}-\frac{1}{M}\sum_{k=1}^{M}x_i^{(k)}\right)^2}\sqrt{\sum_{m=1}^{M}\left(x_j^{(m)}-\frac{1}{M}\sum_{k=1}^{M}x_j^{(k)}\right)^2}} \tag{4}$$

Those two methods are applied because of their ease in high-dimensional uncertainty modeling, but they fail to consider nonlinear correlations and tail dependence among DERs.

2) Vine copula: Vine copula provides an effective method to model high-dimensional complex DS for DERs using pair-copula functions. Based on the C-vine copula, the joint PDF of n input variables $\boldsymbol{X}=(x_1,\ldots,x_n)$ is established as:

$$f(x_1,\ldots,x_n)=\prod_{l=1}^{n}f_l(x_l)\prod_{i=1}^{n-1}\prod_{j=1}^{n-i}c_{i,i+j|\boldsymbol{i}}\left(F(x_i\mid\boldsymbol{x}_i),F(x_{i+j}\mid\boldsymbol{x}_i)\right) \tag{5}$$

In (5), $F(x_i|\boldsymbol{x_i})$ is a conditional CDF of x_i given $\boldsymbol{x_i}$ as:

$$F(x_i\mid\boldsymbol{x}_i)=\frac{\partial C_{i,r|(\sim r,\boldsymbol{i})}\left(F(x_i\mid\boldsymbol{x}_{(\sim r,\boldsymbol{i})}),F(x_{r,\boldsymbol{i}}\mid\boldsymbol{x}_{(\sim r,\boldsymbol{i})})\right)}{\partial F(x_{r,\boldsymbol{i}}\mid\boldsymbol{x}_{(\sim r,\boldsymbol{i})})} \tag{6}$$

Vine copula can depict nonlinear correlations and tail dependence among spatially and temporally correlated DERs. For n input variables, $n(n\text{-}1)/2$ pair copula functions are used to establish the DS and derive the joint PDF [31]. The type of each pair copula function can be determined based on the Akaike's information criterion [32], and the parameters are estimated using the maximum likelihood estimation method [33]. In this paper, LCC and vine copula are used to establish different DSs among DER power injections.

B. Proposed GSA Method for DERs with Various DSs

1) Preliminary of GSA Method: The GSA methods can quantify the impacts of inputs on outputs in power system uncertainty analyses [23]-[29]. For a scalar model response $Y=g(\boldsymbol{X})$ with n inputs $\boldsymbol{X}=(x_1,\ldots,x_n)=(x_i,\boldsymbol{x}_{(\sim i)})$, the variance of Y is decomposed as [27]:

$$D_Y=D_{x_i}\left[E_{\boldsymbol{x}_{(\sim i)}}[g(x_i,\bar{\boldsymbol{x}}_{(\sim i)}\mid x_i)]\right]+E_{x_i}\left[D_{\boldsymbol{x}_{(\sim i)}}[g(x_i,\bar{\boldsymbol{x}}_{(\sim i)}\mid x_i)]\right] \tag{7}$$

Thus, the first-order sensitivity index (FSI) of x_i is defined as:

$$S_i=\frac{D_{x_i}\left[E_{\boldsymbol{x}_{(\sim i)}}[g(x_i,\bar{\boldsymbol{x}}_{(\sim i)})\mid x_i]\right]}{D_Y} \tag{8}$$

Also, the integral representation of FSI is stated as [27]:

$$\begin{aligned}S_i=&\frac{1}{D_Y}\Big[\int f(x_i)\mathrm{d}x_i\Big[\int g(x_i,\bar{\boldsymbol{x}}_{(\sim i)})f(x_i,\bar{\boldsymbol{x}}_{(\sim i)}\big|x_i)\mathrm{d}\bar{\boldsymbol{x}}_{(\sim i)}\\&\times\int g(x_i,\bar{\boldsymbol{x}}'_{(\sim i)})f(x_i,\bar{\boldsymbol{x}}'_{(\sim i)}\big|x_i)\mathrm{d}\bar{\boldsymbol{x}}'_{(\sim i)}\Big]-g_0^2\Big]\end{aligned} \tag{9}$$

$$D_Y=\int\left[g(\boldsymbol{X})\right]^2 f(\boldsymbol{X})\mathrm{d}\boldsymbol{X}-g_0^2$$

Based on two groups of samples $\boldsymbol{X}_a^{(k)}=(x_i^{(k)},\boldsymbol{x}_{(\sim i)}^{(k)})$ and $\boldsymbol{X}_b^{(k)}=(x_i^{(k)},\bar{\boldsymbol{x}}_{(\sim i)}^{(k)})$ $(k=1,\ldots,N_s)$ The Monte Carlo simulation (MCS) is applied to estimate the FSI in (9) as:

$$\begin{cases}\hat{S}_i=\dfrac{\hat{D}_i}{\hat{D}}=\dfrac{1}{\hat{D}}\left[\dfrac{1}{N_s}\sum_{k=1}^{N_s}\left[g\left(\boldsymbol{X}_a^{(k)}\right)g\left(\boldsymbol{X}_b^{(k)}\right)\right]-\hat{g}_0^2\right]\\ \hat{D}=\dfrac{1}{N_s}\sum_{k=1}^{N_s}\left[g\left(\boldsymbol{X}_a^{(k)}\right)\right]^2-\hat{g}_0^2\\ \hat{g}_0=\dfrac{1}{2N_s}\left[\sum_{k=1}^{N_s}g\left(\boldsymbol{X}_a^{(k)}\right)+\sum_{k=1}^{N_s}g\left(\boldsymbol{X}_b^{(k)}\right)\right]\end{cases} \tag{10}$$

Using FSI, GSA methods have been successfully applied to evaluate the impacts of input variables on small-disturbance stability [23], [24], distribution network power flow [25], static voltage stability [26] and maximum MG loadability [27]. However, the GSA methods in the above studies can only evaluate the importance of input variables which are uncorrelated [23], [24] or linearly correlated [25]-[27]. The DER power output features significant nonlinear correlations and tail dependence due to the spatial distribution of DERs and temporal continuity of power outputs. With the increasing penetration of DERs, GSA results would be inaccurate when complex correlations among DERs are ignored. Thus, the impacts of certain uncertainties would be underestimated which might dramatically affect the reliability of power systems.

2) RT-based GSA Method: We propose an RT-based GSA method to quantify the impacts of inputs with complex correlations, which overcomes the shortcomings of existing GSA methods [23]-[29]. For n input variables $\boldsymbol{X}$, the joint PDF of $\boldsymbol{X}$ can be decomposed as:

$$f(\boldsymbol{X})=f(x_1)f(x_2|x_1)f(x_3|x_1,x_2)\ldots f(x_n|\boldsymbol{x_n}) \tag{11}$$

Utilizing (11), RT can transform the correlated inputs $\boldsymbol{X}$ to uncorrelated inputs $\boldsymbol{U}=(u_1,\ldots,u_n)$ that are uniformly distributed over n-dimensional unit hypercube $[0,1]^n$ [31]. Also, $\boldsymbol{U}$ can be transformed to $\boldsymbol{X}$ using inverse RT. The transformation between $\boldsymbol{X}$ and $\boldsymbol{U}$ is stated as:

$$\Gamma:\boldsymbol{X}\mapsto\boldsymbol{U}\qquad\Gamma^{-1}:\boldsymbol{U}\mapsto\boldsymbol{X}$$

$$\begin{cases}u_1=F_1(x_1)\\ u_2=F_{2|1}(x_2|x_1)\\ \quad\vdots\\ u_n=F_{n|\boldsymbol{n}}(x_n|\boldsymbol{x_n})\end{cases}\qquad\begin{cases}x_1=F_1^{-1}(u_1)\\ x_2=F_{2|1}^{-1}(u_2|x_1)\\ \quad\vdots\\ x_n=F_{n|\boldsymbol{n}}^{-1}(u_n|\boldsymbol{x_n})\end{cases} \tag{12}$$

Through RT, the model response Y can be presented as $Y=g(\boldsymbol{X})=h(\boldsymbol{U})$. Thus, FSIs of $\boldsymbol{U}$ can also be defined and estimated using (8) and (10). For FSIs of $\boldsymbol{X}$ and $\boldsymbol{U}$, we have the following propositions.

Proposition 1. The FSI of x_1 for the model response Y is consistent with the FSI of u_1.

Proof. Let us denote $\boldsymbol{U}=(u_1,\boldsymbol{u}_{(\sim 1)})$ and the corresponding input variables $\boldsymbol{X}=(x_1,\boldsymbol{x}_{(\sim 1)})$ based on RT. According to the integral representation of FSI in (9), the FSI of u_1 is stated as:

$$S_1^U=\frac{1}{D_Y}\left[\int\mathrm{d}u_1\left[\int h(u_1,\bar{\boldsymbol{u}}_{(\sim 1)})\mathrm{d}\bar{\boldsymbol{u}}_{(\sim 1)}\times\int h(u_1,\bar{\boldsymbol{u}}'_{(\sim 1)})\mathrm{d}\bar{\boldsymbol{u}}'_{(\sim 1)}-h_0^2\right]\right] \tag{13}$$

Based on RT function Γ: $\boldsymbol{X}\mapsto\boldsymbol{U}$ in (12), we have

$$\mathrm{d}u_1=f(x_1)\mathrm{d}x_1,\quad \mathrm{d}\boldsymbol{u}_{(\sim 1)}=f(\boldsymbol{x}_{(\sim 1)}|x_1)\mathrm{d}\boldsymbol{x}_{(\sim 1)},\quad h_0=g_0 \tag{14}$$

Thus, there is

$$\int h(u_1, \bar{\boldsymbol{u}}_{(\sim 1)}) \mathrm{d}\bar{\boldsymbol{u}}_{(\sim 1)} = \int g(x_1, \bar{\boldsymbol{x}}_{(\sim 1)}) f(\bar{\boldsymbol{x}}_{(\sim 1)} | x_1) \mathrm{d}\bar{\boldsymbol{x}}_{(\sim 1)} \quad (15)$$

Substituting (14) and (15) into (13), the FSI of x_1 is obtained

$$S_1^U = \frac{1}{D_Y}\left[\int f(x_1)\mathrm{d}x_1 \left[\int g(x_1, \bar{\boldsymbol{x}}_{(\sim 1)}) f(x_1, \bar{\boldsymbol{x}}_{(\sim 1)} | x_1)\mathrm{d}\bar{\boldsymbol{x}}_{(\sim 1)} \times \int g(x_1, \bar{\boldsymbol{x}}'_{(\sim 1)}) f(x_1, \bar{\boldsymbol{x}}'_{(\sim 1)} | x_1)\mathrm{d}\bar{\boldsymbol{x}}'_{(\sim 1)}\right] - g_0^2\right] = S_1^X \quad (16)$$

The proof is completed.

Proposition 2. The FSI of $(x_i | \boldsymbol{x}_i)$ (i=2,…,n) for the model response Y is consistent with the FSI of u_i (i=2,…,n).

Proof. Let us denote $x_i'=(x_i|\boldsymbol{x}_i)$ (i=2,…,n) and thus RT realize a one-to-one mapping as:

$$\Gamma' : \boldsymbol{X}' \mapsto \boldsymbol{U} \quad [x_1, x_2', \ldots, x_n'] \mapsto [u_1, u_2, \ldots, u_n] \quad (17)$$

The inputs in $\boldsymbol{X}'$ and $\boldsymbol{U}$ are uncorrelated so the kth samples of $\boldsymbol{X}'$ and $\boldsymbol{U}$ for FSI estimation have the following relationship

$$\begin{aligned} \boldsymbol{U}_a^{(k)} &= \left(u_i^{(k)}, \boldsymbol{u}_{(\sim i)}^{(k)}\right) = \Gamma'\left(x_i'^{(k)}, \boldsymbol{x}_{(\sim i)}'^{(k)}\right) = \Gamma'\left(\boldsymbol{X}_a'^{(k)}\right) \\ \boldsymbol{U}_b^{(k)} &= \left(u_i^{(k)}, \bar{\boldsymbol{u}}_{(\sim i)}^{(k)}\right) = \Gamma'\left(x_i'^{(k)}, \bar{\boldsymbol{x}}_{(\sim i)}'^{(k)}\right) = \Gamma'\left(\boldsymbol{X}_b'^{(k)}\right) \end{aligned} \quad (18)$$

Due to $g\left(\boldsymbol{X}_a'^{(k)}\right) = h\left(\boldsymbol{U}_a^{(k)}\right)$ and $g\left(\boldsymbol{X}_b'^{(k)}\right) = h\left(\boldsymbol{U}_b^{(k)}\right)$, the FSI of u_i can be approximated by using (10) as:

$$S_i^U = \lim_{N_s \to \infty} \hat{S}_i^U = \lim_{N_s \to \infty} \hat{S}_i^{X'} = S_i^{X'}, \quad i = 2, ..., n \quad (19)$$

The proof is completed.

Algorithm 1 Calculate the FSI of x_i by RT-based GSA

1: **Initialization:** Collect the data of input variables $\boldsymbol{X}$ (i.e., DER power output) and determine the model response $Y=g(\boldsymbol{X})$ (i.e., PVUF);
2: Establish the probability models of $\boldsymbol{X}$ with spatial and temporal correlations based on the uncertainty modeling in Section III-A;
3: **for** i = 1 to n **do**
4: Set the ith permutation $\boldsymbol{X}^{(i)}=(x_i,x_{i+1},\ldots,x_n,x_1,\ldots,x_{i-1})$;
5: **if** LCC matrix is used to depict the DS in $\boldsymbol{X}^{(i)}$ **then**
6: Derive the conditional CDFs for RT in (12) by using Nataf transformation as detailed in [30];
7: **end if**
8: **if** vine copula is used to depict the DS in $\boldsymbol{X}^{(i)}$ **then**
9: Derive the conditional CDFs for RT in (12) by using (6);
10: **end if**
11: Build the relationship between $\boldsymbol{X}^{(i)}$ and $\boldsymbol{U}$ through RT and obtain the model response $Y=g(\boldsymbol{X}^{(i)})=h(\boldsymbol{U})$;
12: Generate two groups of uncorrelated samples of $\boldsymbol{U}$ which are denoted as $\boldsymbol{U}_a^{(k)} = (u_1^{(k)}, \boldsymbol{u}_{(\sim 1)}^{(k)})$ and $\boldsymbol{U}_b^{(k)} = (u_1^{(k)}, \bar{\boldsymbol{u}}_{(\sim 1)}^{(k)})$ (k=1,…,N_s) by utilizing Uniform distribution;
13: Obtain the corresponding two groups of samples of Y denoted as $h(\boldsymbol{U}_a^{(k)})$ and $h(\boldsymbol{U}_b^{(k)})$ (k=1,…,N_s) by using $Y=g(\boldsymbol{X}^{(i)})=h(\boldsymbol{U})$ in step 11;
14: Substitute the samples $h(\boldsymbol{U}_a^{(k)})$ and $h(\boldsymbol{U}_b^{(k)})$ (k=1,…,N_s) into (10) to calculate the FSI of u_1 which is the FSI of x_i;
15: **end for**
16: **Results:** FSIs of $x_1,\ldots,x_n$

The FSI of u_1 is unconditional which is equal to the FSI of x_1. Thus, the FSI of u_1 can be directly used to evaluate the impacts of x_1 and the correlations of x_1 with other inputs ($x_2,\ldots,x_n$) on the variation of Y. The FSI of u_i (i=2,…,n) is conditional, which does not consider the impacts of correlations of x_i and $\boldsymbol{x}_i$ on the variation of Y. The corresponding relationship of FSIs in **Propositions 1** and **2** is related to the permutation of inputs in $\boldsymbol{X}$. There are n! permutations of inputs in $\boldsymbol{X}$ and we can obtain various FSIs by changing the order of inputs. Considering n DERs as inputs $\boldsymbol{X}$ in ADN, **Algorithm 1** presents the process of calculating FSIs of $x_1,\ldots,x_n$ using n permutations of $\boldsymbol{X}$. Also, two other RT-GSA indices are defined to represent the impacts of $\boldsymbol{X}$ on Y as follows:

1. *Uncorrelated sensitivity index (USI):* USI of x_i is defined as the FSI of u_n which corresponds to the FSI of $(x_i|\boldsymbol{x}_{(\sim i)})$. The USI quantifies the single impacts of x_i on the variation of Y without considering the impacts of correlations of x_i with other inputs $\boldsymbol{x}_{(\sim i)}$. The USI of x_i can be stated as:
$$S_{\mathrm{U},i}^{\boldsymbol{X}} = S_n^U \quad (20)$$
2. *Correlated sensitivity index (CSI):* CSI is used to quantify the impacts of correlations among x_i and $\boldsymbol{x}_{(\sim i)}$ on the variation of Y, which is defined as:
$$S_{\mathrm{C},i}^{\boldsymbol{X}} = S_i^{\boldsymbol{X}} - S_{\mathrm{U},i}^{\boldsymbol{X}} \quad (21)$$

The USI of x_i can be obtained by calculating the FSI of u_n with the permutation $\boldsymbol{X}^{(i+1)}=(x_{i+1},x_{i+2},\ldots,x_n,x_1,\ldots,x_i)$. The calculation of FSI for u_n is similar to the calculation of FSI for u_1 in **Algorithm 1**. Thus, the CSI of x_i can be derived using the FSI and USI of x_i as (21). In this paper, FSI, USI, and CSI are combined to evaluate the impacts of variable DER power injection with complex correlations on PVUF. The conditional CDFs in RT is vital for applying the RT-based GSA method. Considering the probability models of inputs, LLC and vine copula can be both handled to derive the conditional CDFs using the RT-based GSA method as shown in **Algorithm 1**. Thus, compared with the GSA methods in [23]-[29], the proposed RT-based GSA method is applicable to quantify the impacts of DERs with various DSs on VU.

IV. Stage Two: Unbalance Mitigation

In this section, an optimal mitigation strategy for DER power injection is proposed by allocating a limited number of ESDs. Thus, the risk of exceeding VUF limit can be decreased by using ESDs to compensate the fluctuations in identified critical DER power injections.

A. Determining the Allocation of ESDs

In a time window, ESDs can be used to mitigate VU by reducing the fluctuation in DER power injection as shown in Fig. 3. After allocating ESDs, the variation range of DER power injection is diminished so that the risk of exceeding VUF limit is decreased. However, in practical power systems, the available ESDs might be limited [34] or the ESDs are unavailable due to the geographical distribution of DERs. In this paper, we consider two kinds of ESDs: shared fixed ESDs (FESDs) and mobile ESDs (MESDs) [35]. The FESD is shared among several DERs. By closing the corresponding switch, the shared FESD is allocated at a certain DER bus to compensate the fluctuation in DER power injection. Compared with the FESDs, the MESDs are more flexible which can be allocated at

This article has been accepted for publication in a future issue of this journal, but has not been fully edited. Content may change prior to final publication. Citation information: DOI 10.1109/TSTE.2020.2992960, IEEE Transactions on Sustainable Energy

any DER buses to compensate the fluctuation in DER power injection while the operation costs of MESDs would be higher.

In this paper, FESDs and MESDs are considered to mitigate VU in ADN by reducing the fluctuation in DER power injection. In Stage one, the proposed RT-based GSA method quantifies the impacts of variable DERs on PVUF and derives a priority ranking (PR) of DERs based on the RT-GSA indices. Then, the ESDs are allocated at the critical DER buses according to the PR of DERs. As shown in Fig. 4, DER_2, DER_3, and DER_4 are identified as critical DERs which have significant impacts on VU. Thus, the shared $FESD_1$ between DER_1 and DER_2 is preferentially integrated into ADN at the DER_2 bus by closing the switch S_2. Also, $MESD_1$ and $MESD_2$ are allocated at the buses of DER_3 and DER_4, respectively. For DER_1 and DER_5, their impacts on VU are insignificant so ESDs are not allocated. The results of Stage one determine the allocation of ESDs to furthest mitigate VU by using the limited number of ESDs.

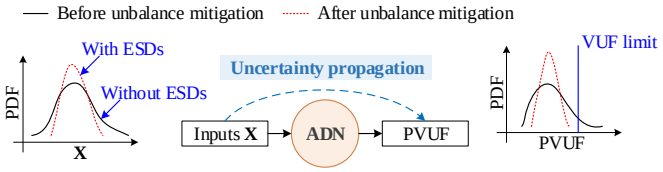

Fig. 3. Mitigating the unbalance using ESDs.

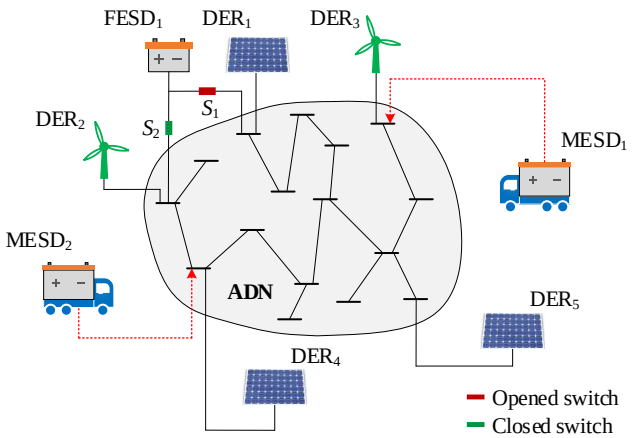

Fig. 4. Allocation of FESDs and MESDs in ADN.

B. Mitigation Strategy for Variable DER Power Injection

After allocating ESDs at critical DERs buses, the optimal mitigation strategy is proposed to compensate the fluctuations of DER power injections by charging and discharging of ESDs. The corresponding optimal mitigation problem is formulated in (22.1)-(22.10). Here, the utilized ESDs can be fixed or mobile. Based on the probability models of DERs in Section III-A, N scenes for the power injection of DER_i with spatial and temporal correlations are generated in a time window with T time instants.

$$\min \sum_{m=1}^{N}\sum_{t=1}^{T}\left(P_{m,t}^{\mathrm{DER}_i}-\bar{P}_m\right)^2 \tag{22.1}$$

Subject to:

$$\bar{P}_m=\frac{1}{T}\sum_{t=1}^{T}P_{m,t}^{\mathrm{DER}_i},\ \forall m \tag{22.2}$$

$$P_{m,t}^{\min}\le P_{m,t}^{\mathrm{DER}_i}\le P_{m,t}^{\max},\ \forall m,\forall t \tag{22.3}$$

$$P_{m,t}^{\mathrm{DER}_i}=P_{m,t}^{\mathrm{D}}-\Delta P_{m,t}^{\mathrm{c}}+\Delta P_{m,t}^{\mathrm{disc}},\ \forall m,\forall t \tag{22.4}$$

$$SOC_{m,t}=SOC_{m,t-1}+\eta_{\mathrm{c}}\Delta P_{m,t}^{\mathrm{c}}-\eta_{\mathrm{disc}}\Delta P_{m,t}^{\mathrm{disc}},\ \forall m,\forall t \tag{22.5}$$

$$SOC_{\min}\le SOC_{m,t}\le SOC_{\max},\ \forall m,\forall t \tag{22.6}$$

$$u_{m,t}^{\mathrm{c}}+u_{m,t}^{\mathrm{disc}}\le 1,\ \forall m,\forall t \tag{22.7}$$

$$0\le\Delta P_{m,t}^{\mathrm{c}}\le u_{m,t}^{\mathrm{c}}\Delta P_{\max}^{\mathrm{c}},\ \forall m,\forall t \tag{22.8}$$

$$0\le\Delta P_{m,t}^{\mathrm{disc}}\le u_{m,t}^{\mathrm{disc}}\Delta P_{\max}^{\mathrm{disc}},\ \forall m,\forall t \tag{22.9}$$

$$SOC_{m,0}=\tau,\ \forall m \tag{22.10}$$

In the above model, the objective (22.1) is to minimize the variance of DER_i power injection after allocating the ESD. Constraint (22.2) represents the mean of DER_i power injection within the time window [1, T] in the mth scene. Constraint (22.3) describes the limit of DER_i power injection after allocating the ESD. Constraint (22.4) represents the power balance after charging or discharging of ESD. Constraints (22.5)-(22.6) represent the ESD capacity balance and limit, respectively. Constraint (22.7) ensures that the ESD would not charge and discharge simultaneously. Constraints (22.8)-(22.9) limit the charging and discharging power, respectively. Constraint (22.10) depicts the initial state-of-charge of ESD in each scene.

V. Case Study

A. ADN System Description

The effectiveness of the proposed two-stage UQUM method is verified using a 123-bus three-phase unbalanced ADN system. There are six renewable DERs integrated into the 123-bus ADN system, including three PV cells (DER_2, DER_3, DER_6) and three wind turbines (DER_1, DER_4, DER_5). DER_1-DER_6 are integrated into the ADN at buses 19 (Phase A), 73 (Phase C), 99 (Phase B), 32 (Phase C), 66 (Phase C), 107 (Phase B), respectively. The original data of DER power output is extracted from NREL Solar and Wind Integration datasets and we increase the DER power outputs proportionally. Four uncorrelated Normal distribution functions with 10% standard deviation are used to depict load uncertainties within four sub-regions of ADN. The variable DER power injections and loads are concerned as input variables in the studied ADN.

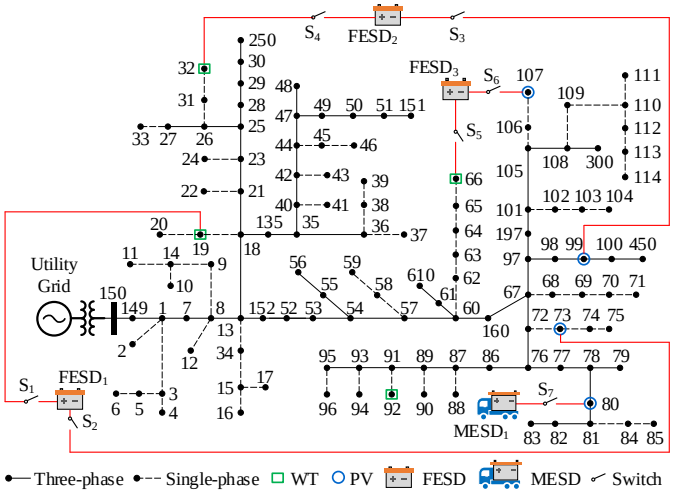

Fig. 5. A 123-bus three-phase unbalanced ADN system.

In Stage one, the proposed RT-GSA method is applied to quantify the impacts of correlated DERs on VU and identify critical DERs. MCS with 10,000 samples is used to calculate the RT-GSA indices of DERs and loads. The applicability of

This article has been accepted for publication in a future issue of this journal, but has not been fully edited. Content may change prior to final publication. Citation information: DOI 10.1109/TSTE.2020.2992960, IEEE Transactions on Sustainable Energy

RT-based GSA for DERs with various DSs (LCC and vine copula) is demonstrated and the impacts of complex correlations on VU are studied. In Stage two, the optimal mitigation strategy is adopted to mitigate VU by allocating FESDs and MESDs at critical DER buses. The locations of ESDs and DERs in the studied 123-bus three-phase unbalanced ADN system are shown in Fig. 5. The programs are performed with Matlab 2018a on a PC with Intel Core i5-8500 3.00GHz CPU and 8GB of RAM. The optimal model in Stage two is solved by GUROBI 8.1.1.

B. Stage One of UQUM

1) Applicability of RT-based GSA for DERs with Various DSs: We select a dataset of six DERs in a time window with 48 time instants from 8:00 to 12:00 A.M. The corresponding distributions and LLC matrix $\boldsymbol{\rho}$ of six DERs are presented in Fig. 6, where orange subfigures represent PDFs of power outputs of participating DERs, and blue subfigures represent nonlinear correlations and the strong tail dependence among participating DERs.

In this part, two DSs including LCC and vine copula are applied to describe the correlation of DER power outputs. As discussed in Section II, LCC which is usually used to describe the linear correlation and vine copula is superior in depicting nonlinear correlations and tail dependences. With the two DSs, the probability models of DERs are established and uncertainty is propagated through the ADN system. Bus 83 with severe VU is selected as an observation point and GSA method is performed to quantify the impacts of variable DERs on the PVUF at bus 83. The FSIs of inputs with different DSs are given in Table I based on the GSA methods [25]-[27] and the RT-based GSA method, respectively. $\text{Load}_{1\text{-}4}$ stands for a group of four uncorrelated Normal inputs which depict load uncertainties within the four sub-regions of ADN.

TABLE I
FSIs OF INPUTS WITH VARIOUS DSs BY TWO GSA METHODS

Input variable	GSA methods in [25]-[27]		RT-based GSA method	
	LCC	Vine copula	LCC	Vine copula
DER_1	0.003	—	0.003	0.002
DER_2	0.881	—	0.881	0.901
DER_3	0.617	—	0.617	0.580
DER_4	0.032	—	0.032	0.022
DER_5	0.004	—	0.004	0.008
DER_6	0.755	—	0.755	0.788
$\text{Load}_{1\text{-}4}$	0.004	—	0.004	0.003

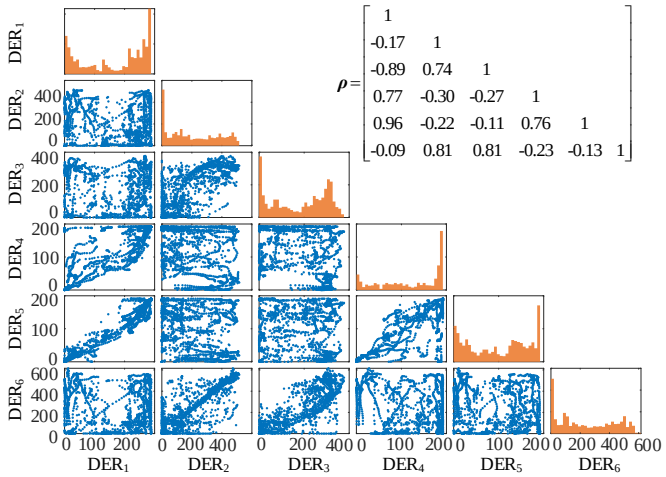

Fig. 6. Distributions of power outputs (kW) of correlated DERs.

In Table I, for the inputs with LCC-based DS, the results obtained by GSA methods in [25]-[27] and RT-based GSA method are the same, which verifies the effectiveness of the proposed method. For the inputs with vine copula-based DS, the GSA method results are unavailable in [25]-[27] while the RT-based GSA method derives the FSIs to quantify the impacts of inputs on PVUF at bus 83. Compared with the existing GSA methods in [25]-[27], the proposed RT-based GSA method is more general in practical applications due to its applicability for various DSs. The identified critical DERs (DER_2, DER_3, and DER_6) are the same considering the inputs with LCC-based DS or vine copula-based DS. It implies that the impacts of nonlinear correlations and tail dependence among inputs for identifying critical inputs are insignificant in this example.

Furthermore, we select a dataset of these six DERs in a time window with 48 time instants from 3:00 to 7:00 P.M. For the inputs with LCC-based DS, the GSA methods in [25]-[27] are unavailable because the LCC matrix of inputs is not positive definite after using Nataf transformation. For the inputs with vine copula-based DS, the proposed RT-based GSA method can be applied to quantify the impacts of DERs and obtain the critical DERs. Based on the proposed RT-based GSA method, the FSIs and PR of DERs are derived as presented in Table II. It can be seen that DER_2 has the most significant impacts on PVUF at 83 and the impacts of $\text{Load}_{1\text{-}4}$ are negligible.

TABLE II
FSIs AND PR OF INPUTS BASED ON THE RT-GSA METHOD

	DER_1	DER_2	DER_3	DER_4	DER_5	DER_6	$\text{Load}_{1\text{-}4}$
FSI	0.259	0.501	0.398	0.483	0.457	0.191	0.002
PR	5th	1st	4th	2nd	3rd	6th	8th

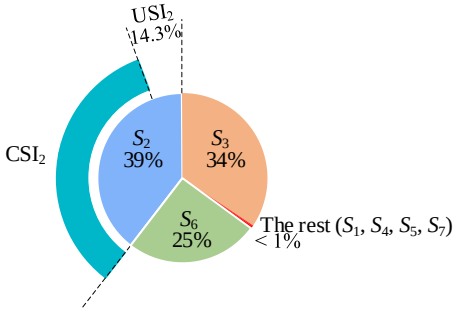

Fig. 7. Quantifying the impacts of correlations of DER_2 and other DERs.

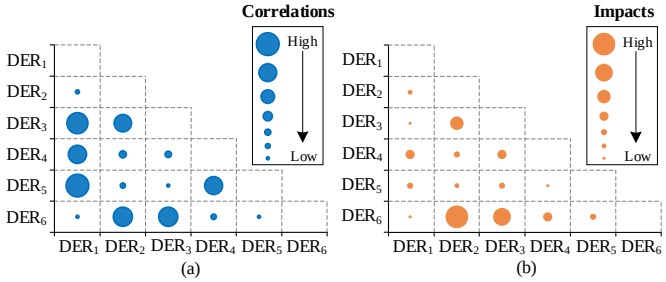

Fig. 8. Comparisons of (a) correlations of different DERs and (b) impacts of those correlations on PVUF at bus 83.

2) Impacts of DER Correlations on VU: According to the FSIs of inputs with vine copula-based DS, the DER_2 has the largest impacts on the PVUF at bus 83 while the impacts of DER_1 are most insignificant. DER_2, DER_3, and DER_6 are identified as critical inputs because their FSIs are much larger than the FSIs of others. Further, the UFIs and CSIs defined in Section III-B

This article has been accepted for publication in a future issue of this journal, but has not been fully edited. Content may change prior to final publication. Citation information: DOI 10.1109/TSTE.2020.2992960, IEEE Transactions on Sustainable Energy

are utilized to quantify the impacts of correlated DERs on VU. It should be noted that $Load_{1\text{-}4}$ is uncorrelated with other inputs. Fig. 7 shows the proportion of FSIs of the inputs and quantifies the impacts of correlations of DER_2 and other DERs on the PVUF at bus 83. Meanwhile, S_1-S_7 stand for the FSIs of inputs (DER_1-DER_6, $Load_{1\text{-}4}$). USI_2 and CSI_2 represent the single impacts of DER_2 and the impacts of correlations of DER_2 and other DERs on the PVUF at bus 83, respectively. The proportion of USI_2 is 14.3%, which indicates that the single impacts of DER_2 are less than the impacts of correlations of DER_2 and other DERs.

Fig. 8 presents the correlations of two different DERs and the impacts of those correlations on PVUF. Strong correlations exist in several groups of bivariate (such as DER_1 and DER_3, DER_1 and DER_4, DER_2 and DER_6). However, only the impacts of correlations of DER_2 and DER_6 and of DER_3 and DER_6 are significant. The results indicate that the impacts of correlations on the PVUF variation might be minor though the correlations are strong.

C. Stage Two of UQUM

In this part, we design two scenarios for VU mitigation by allocating ESDs as introduced in Section IV. In scenario one, only three shared FESDs ($FESD_1$ shared between DER_1 and DER_2; $FESD_2$ shared between DER_3 and DER_4; $FESD_3$ shared between DER_5 and DER_6) are considered for VU mitigation. In scenario two, two additional DERs (DER_7 and DER_8) are integrated into the ADN at buses 80 (Phase B) and 92 (Phase C). Besides the three FESDs, MESDs can be used to alleviate VU in scenario two. In Table III, seven cases are conducted to illustrate the effects of unbalance mitigation by allocating ESDs.

TABLE III
MITIGATING THE UNBALANCE USING FESDS AND MESDS

Scenario	Case	Allocation of ESDs
Scenario one (only considering FESDs)	Case 1	Without allocating any FESDs.
	Case 2	$FESD_1$, $FESD_2$, and $FESD_3$ are allocated at DER_1, DER_4, and DER_5, respectively.
	Case 3	$FESD_1$, $FESD_2$, and $FESD_3$ are allocated at DER_2, DER_3, and DER_6, respectively.
Scenario two (considering both FESDs and MESDs)	Case 4	Without allocating any ESDs.
	Case 5	$FESD_1$, $FESD_2$, and $FESD_3$ are allocated at DER_2, DER_3, and DER_6, respectively.
	Case 6	$MESD_1$ is allocated at DER_7.
	Case 7	$MESD_1$ and $FESD_3$ are allocated at DER_7 and DER_6, respectively.

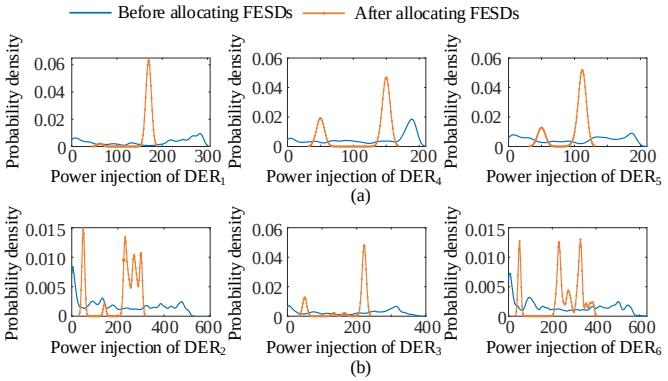

Fig. 9. PDFs of DER power injection (kW) before and after allocating the FESDs in (a) Case 2 and (b) Case 3.

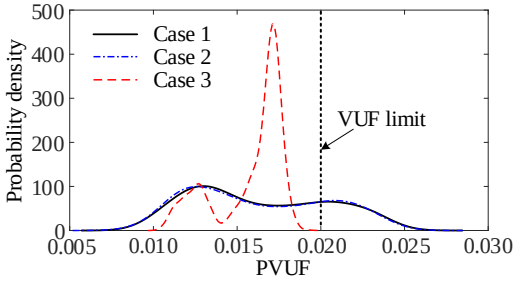

Fig. 10. PDFs of PVUF at bus 83 in scenario one.

In scenario one, we compare the effects of mitigating the unbalance at bus 83 by allocating FESDs at different DER buses. In Table I, the results of Stage one indicate that the impacts of DER_1, DER_4, and DER_5 on the variation of PVUF at bus 83 are insignificant and DER_2, DER_3, and DER_6 are the critical DERs. Accordingly, in Case 2, the FESDs are allocated to buses with less critical DERs (DER_1, DER_4, and DER_5). In Case 3, the FESDs are allocated to buses of critical DERs (DER_2, DER_3, and DER_6). Fig. 9 presents the PDFs of DER power injections before and after allocating FESDs. Fig. 10 presents the PDFs of PVUF at bus 83 in scenario one.

In Fig. 9, after allocating FESDs, the variation of each DER power injection is reduced and the DER power injection is mainly distributed around certain values in both Cases 2 and 3. However, the effects of VU mitigation by allocating FESDs are greatly different in Cases 2 and 3 as shown in Fig. 10. In Case 2, fluctuations in DER_1, DER_4, and DER_5 are reduced while the PDF of PVUF at bus 83 is almost the same as that in Case 1 where the PVUF exceeds the VUF limit (2%) with a 24.61% probability. In Case 3, the effects of VU mitigation are significant in which the PVUF variation is regulated within a safe range by allocating the FESDs at critical DERs. The comparison of Cases 2 and 3 verifies the effectiveness of the RT-based GSA method on identifying the critical DERs.

In scenario two, two additional DERs (i.e., DER_7 and DER_8) are integrated into the ADN. Here, we choose bus 160 with severe VU as the observation point and the data of eight DERs includes 48 time instants from 1:00 to 4:00 P.M. In Stage one, the RT-based GSA method is performed to quantify the impacts of DERs with vine copula-based DS on the PVUF at bus 160. Also, the GSA methods in [25]-[27] is applied considering the DERs with LCC-based DS. The FSIs of DERs are obtained in Stage one and the PR of DERs are given in Table IV, where DER_7, DER_6, DER_3, and DER_2 are identified as the critical DERs with the PR 1st-4th.

Four cases (Cases 4-7) in Table III are conducted to illustrate the effects of mitigating the unbalance. The power injection of DER_7 is the most critical factor for the variation of PVUF. Fig. 11 presents the PDFs of PVUF at bus 160 for the four cases. In Case 5, only three FESDs are used to compensate the fluctuation in DER_6, DER_3, and DER_2, which are the critical DERs with the PR 2nd-4th. Compared with the PDF in Case 4, the variance of PVUF in Case 5 is decreased after allocating three FESDs while the PVUF at bus 160 still exceeds the VUF limit with a 4.76% probability. In Case 6, MESDs is flexible to be integrated at the DER_7 bus with the most critical factor. In Fig. 11, the variation range of PVUF at bus 160 only exceeds the VUF limit with a lower probability of 1.05% as compared with that in Cases 4 and 5. In Case 7, $MESD_1$ and $FESD_3$ are

allocated at DER_7 and DER_6 with the PR 1st and 2nd, respectively. Compared with Case 6, VU in Case 7 is further alleviated and the corresponding PVUF is regulated within a safe range. Thus, the MESDs and FESDs can be coordinated to reduce the impacts of variable DER power injections on VU. The PR of DERs obtained in Stage one is used to guide the allocation of MESDs and FESDs in VU mitigation.

TABLE IV
FSIs AND PR OF DERs

	DER_1	DER_2	DER_3	DER_4	DER_5	DER_6	DER_7	DER_8
FSI^1	0.001	0.094	0.127	0.049	0.003	0.256	0.395	0.002
PR	8th	4th	3rd	5th	6th	2nd	1st	7th
FSI^2	0.016	0.090	0.168	0.035	0.011	0.251	0.413	0.001
PR	6th	4th	3rd	5th	7th	2nd	1st	8th

*FSI^1 represents the FSIs obtained by RT-GSA method with vine copula-based DS; FSI^2 represents the FSIs obtained by GSA methods in [25]-[27] with LCC-based DS.

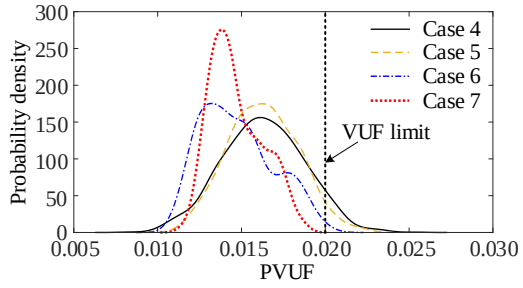

Fig. 11. PDFs of PVUF at bus 160 in scenario two.

VI. CONCLUSION

This paper proposes a two-stage UQUM framework to quantify the impacts of variable DERs on VU in ADN and mitigate the corresponding impacts by dispatching available ESDs. In Stage one, the RT-based GSA method is proposed to quantify the impacts of correlated DERs on PVUF and identify critical DERs with significant impacts on VU. In Stage two, the joint allocation of available FESDs and MESDs is proposed to compensate the fluctuations of identified critical DERs for alleviating VU with enhanced efficiency.

The proposed two-stage UQUM framework presents the following salient features:

1. Compared with the existing GSA methods presented in [25]-[27], the proposed RT-based GSA method is capable of handling the DERs with complex DS established by vine copula and identifying the critical DERs. In practical applications, the proposed RT-based GSA method is more general to quantify the impacts of input variables with various DSs.
2. The effectiveness of the proposed UQUM framework for mitigating VU is verified by allocating the available ESDs at the critical DER buses and developing the optimal mitigation strategy.
3. The joint allocation of FESDs and MESDs provides more flexible approaches to effectively alleviate the impacts of variable DER power injections on VU in ADN.

Our future work will focus on the application of uncertainty quantification methods in the scheduling of MESDs and EVs to improve the resilience and reliability of power systems.

REFERENCES

[1] Y. Liu, J. Li, and L. Wu, "Coordinated optimal network reconfiguration and voltage regulator/der control for unbalanced distribution systems," *IEEE Trans. Smart Grid*, vol. 10, no. 3, pp. 2912-2922, May 2019.

[2] Q. Zhou, M. Shahidehpour, A. Alabdulwahab and A. Abusorrah, "Privacy-preserving distributed control strategy for optimal economic operation in islanded reconfigurable microgrids," *IEEE Trans. Power Syst.*, early access, doi: 10.1109/TPWRS.2020.2985995.

[3] Y. Kim, "Development and analysis of a sensitivity matrix of a three-phase voltage unbalance factor," *IEEE Trans. Power Syst.*, vol. 33, no. 3, pp. 3192-3195, May 2018.

[4] Y. Wang, N. Zhang, H. Li, J. Yang, and C. Kang, "Linear three-phase power flow for unbalanced active distribution networks with PV nodes," *CSEE J. Power Energy Syst.*, vol. 3, no. 3, pp. 321-324, Sep. 2017.

[5] Q. Zhou, M. Shahidehpour, A. Alabdulwahab, and A. Abusorrah, "A cyber-attack resilient distributed control strategy in islanded microgrids," *IEEE Trans. Smart Grid*, early access, doi: 10.1109/TSG.2020.2979160.

[6] Q. Zhou, M. Shahidehpour, A. Abdulwhab, and A. M. Abusorrah, "Unification scheme for managing master controller failures in networked microgrids," *IEEE Trans. Power Syst.*, early access, doi: 10.1109/TPWRS.2019.2958643.

[7] K. H. Chua, Y. S. Lim, P. Taylor, S. Morris, and J. Wong, "Energy storage system for mitigating voltage unbalance on low-voltage networks with photovoltaic systems," *IEEE Trans. Power Del.*, vol. 27, no. 4, pp. 1783-1790, Oct. 2012.

[8] F. Shahnia, P. J. Wolfs, and A. Ghosh, "Voltage unbalance reduction in low voltage feeders by dynamic switching of residential customers among three phases," *IEEE Trans. Smart Grid*, vol. 5, no. 3, pp. 1318-1327, May 2014.

[9] T. Chen and J. Cherng, "Optimal phase arrangement of distribution transformers connected to a primary feeder for system unbalance improvement and loss reduction using a genetic algorithm," *IEEE Trans. Power Syst.*, vol. 15, no. 3, pp. 994-1000, Aug. 2000.

[10] S. Martinenas, K. Knezović, and M. Marinelli, "Management of power quality issues in low voltage networks using electric vehicles: experimental validation," *IEEE Trans. Power Del.*, vol. 32, no. 2, pp. 971-979, Apr. 2017.

[11] S. Weckx and J. Driesen, "Load balancing with EV chargers and PV inverters in unbalanced distribution grids," *IEEE Trans. Sustain. Energy*, vol. 6, no. 2, pp. 635-643, Apr. 2015.

[12] M. Savaghebi, A. Jalilian, J. C. Vasquez, and J. M. Guerrero, "Secondary control scheme for voltage unbalance compensation in an islanded droop-controlled microgrid," *IEEE Trans. Smart Grid*, vol. 3, no. 2, pp. 797-807, Jun. 2012.

[13] M. Zeraati, M. E. H. Golshan, and J. M. Guerrero, "Voltage quality improvement in low voltage distribution networks using reactive power capability of single-phase PV inverters," *IEEE Trans. Smart Grid*, vol. 10, no. 5, pp. 5057-5065, Sep. 2019.

[14] M. Hamzeh, H. Karimi, and H. Mokhtari, "Harmonic and negative-sequence current control in an islanded multi-bus MV microgrid," *IEEE Trans. Smart Grid*, vol. 5, no. 1, pp. 167–176, Jan. 2014.

[15] M. J. E. Alam, K. M. Muttaqi, and D. Sutanto, "Community energy storage for neutral voltage rise mitigation in four-wire multigrounded LV feeders with unbalanced solar PV allocation," *IEEE Trans. Smart Grid*, vol. 6, no. 6, pp. 2845-2855, Nov. 2015.

[16] M. J. E. Alam, K. M. Muttaqi, and D. Sutanto, "Alleviation of neutral-to-ground potential rise under unbalanced allocation of rooftop PV using distributed energy storage," *IEEE Trans. Sustain. Energy*, vol. 6, no. 3, pp. 889-898, Jul. 2015.

[17] Q. Zhou, M. Shahidehpour, A. Alabdulwahab, and A. M. Abusorrah, "Flexible division and unification control strategies in networked microgrids for resilience enhancement," *IEEE Trans. Power Syst.*, vol. 35, no. 1, pp. 474-486, Jan. 2020.

[18] Q. Zhou, Z. Tian, M. Shahidehpour, X. Liu, A. Alabdulwahab, and A. M. Abusorrah, "Optimal consensus-based distributed control strategy for coordinated operation of networked microgrids," *IEEE Trans. Power Syst.*, vol. 35, no. 3, pp. 2452-2462, May 2020.

[19] Z. Liu and J. V. Milanović, "Probabilistic estimation of voltage unbalance in MV distribution networks with unbalanced load," *IEEE Trans. Power Del.*, vol. 30, no. 2, pp. 693-703, Apr. 2015.

[20] G. Gruosso, R. Netto, L. Daniel, and P. Maffezzoni, "Joined probabilistic load flow and sensitivity analysis of distribution networks based on polynomial chaos method," *IEEE Trans. Power Syst.*, vol. 35, no. 1, pp. 618-627, Jan. 2020.

[21] N. C. Woolley and J. V. Milanovic, "Statistical estimation of the source and level of voltage unbalance in distribution networks," *IEEE Trans. Power Del.*, vol. 27, no. 3, pp. 1450-1460, Jul. 2012.
[22] Yaw-Juen Wang and L. Pierrat, "A method integrating deterministic and stochastic approaches for the simulation of voltage unbalance in electric power distribution systems," *IEEE Trans. Power Systems*, vol. 16, no. 2, pp. 241-246, May 2001.
[23] R. Preece and J. V. Milanović, "Assessing the applicability of uncertainty importance measures for power system studies," *IEEE Trans. on Power Syst.*, vol. 31, no. 3, pp. 2076-2084, May 2016.
[24] K. N. Hasan, R. Preece, and J. V. Milanović, "Priority ranking of critical uncertainties affecting small-disturbance stability using sensitivity analysis techniques," *IEEE Trans. Power Syst.*, vol. 32, no. 4, pp. 2629-2639, Jul. 2017.
[25] F. Ni, M. Nijhuis, P. H. Nguyen, and J. F. G. Cobben, "Variance-based global sensitivity analysis for power systems," *IEEE Trans. Power Syst.*, vol. 33, no. 2, pp. 1670-1682, Mar. 2018.
[26] X. Xu, Z. Yan, M. Shahidehpour, H. Wang, and S. Chen, "Power system voltage stability evaluation considering renewable energy with correlated variabilities," *IEEE Trans. Power Syst.*, vol. 33, no. 3, pp. 3236-3245, May 2018.
[27] X. Xu, Z. Yan, M. Shahidehpour, S. Chen, H. Wang, Z. Li, and Q. Zhou, "Maximum loadability of islanded microgrids with renewable energy generation," *IEEE Trans. Smart Grid*, vol. 10, no. 5, pp. 4696-4705, Sep. 2019.
[28] H. Wang, Z. Yan, X. Xu, and K. He, "Probabilistic power flow analysis of microgrid with renewable energy," *Int. J. Electr. Power Energy Syst.*, early access, doi: 10.1016/J.IJEPES.2019.105393.
[29] H. Wang, Z. Yan, M. Shahidehpour, X. Xu, and Q. Zhou, "Quantitative evaluations of uncertainties in multivariate operations of microgrids," *IEEE Trans. Smart Grid*, early access, doi: 10.1109/TSG.2020. 2971689.
[30] R. Lebrun and A. Dutfoy, "An innovating analysis of the Nataf transformation from the copula viewpoint," *Probab. Eng. Mech.*, vol. 24, no. 3, pp. 312-320, Jul. 2009.
[31] E. Torre, S. Marelli, P. Embrechts, and B. Sudret, "A general framework for data-driven uncertainty quantification under complex input dependencies using vine copulas," *Probab. Eng. Mech.*, vol. 55, pp. 1-16, Jan. 2019.
[32] H. V. Haghi and S. Lotfifard, "Spatiotemporal modeling of wind generation for optimal energy storage sizing," *IEEE Trans. Sustain. Energy*, vol. 6, no. 1, pp. 113-121, Jan. 2015.
[33] M. Sun, I. Konstantelos, and G. Strbac, "C-vine copula mixture model for clustering of residential electrical load pattern data," *IEEE Trans. Power Syst.*, vol. 32, no. 3, pp. 2382-2393, May 2017.
[34] D. Han, C. Zhang, J. Ping, and Z. Yan, "Smart contract architecture for decentralized energy trading and management based on blockchains," *Energy*, early access, doi: 10.1016/j.energy.2020.117417.
[35] Q. Zhou, M. Shahidehpour, M. Yan, X. Wu, A. Alabdulwahab, and A. M. Abusorrah, "Distributed secondary control for islanded microgrids with mobile emergency resources," *IEEE Trans. Power Syst.*, vol. 35, no. 2, pp. 1389-1399, Mar. 2020.

BIOGRAPHIES

Han Wang (S'19) received the B.S. degree in electrical engineering from Zhejiang University, Hangzhou, China, in 2015. He is currently pursuing the Ph.D. degree in the Department of Electrical Engineering at Shanghai Jiao Tong University, Shanghai, China. He is also a Visiting Scholar with the Robert W. Galvin Center for Electricity Innovation, Illinois Institute of Technology, Chicago, IL, USA. His research interests include microgrid operation and power system uncertainty analysis.

Zheng Yan received the B.S. degree from Shanghai Jiao Tong University, Shanghai, China, in 1984 and the M.S. and Ph.D. degrees from Tsinghua University, Beijing, China, in 1987 and 1991, respectively, all in electrical engineering. He is a Professor of electrical engineering from Shanghai Jiao Tong University. His current research interests include application of optimization theory to power systems, power markets, and dynamic security assessment.

Mohammad Shahidehpour (F'01) received an Honorary Doctorate degree in electrical engineering from the Polytechnic University of Bucharest, Bucharest, Romania. He is the Bodine Chair Professor and Director of the Robert W. Galvin Center for Electricity Innovation at Illinois Institute of Technology, Chicago, IL, USA. Dr. Shahidehpour is a member of the US National Academy of Engineering and a Fellow of IEEE, the American Association for the Advancement of Science (AAAS), and the National Academy of Inventors (NAI).

Quan Zhou (SM'19) received the B.S. and M.S. degrees from the Department of Electrical Engineering, Shanghai Jiao Tong University, Shanghai, China, in 2011 and 2016, respectively. He received the Ph.D. degree from Illinois Institute of Technology, Chicago, IL, USA, in 2019. He is currently a Senior Research Associate in the Robert W. Galvin Center for Electricity Innovation at Illinois Institute of Technology. His research interests include microgrid operation and control, cyber-physical systems, 5G wireless communications, smart cities, and energy economics.

Xiaoyuan Xu (S'15-M'16) received both the B.S. and Ph.D. degrees in electrical engineering from Shanghai Jiao Tong University, Shanghai, China, in 2010 and 2016, respectively. He was a Visiting Scholar with the Robert W. Galvin Center for Electricity Innovation, Illinois Institute of Technology, Chicago, IL, USA, from 2017 to 2018. He is currently an Assistant Professor with Shanghai Jiao Tong University. His research interests include power system uncertainty quantification and power system optimization.